LightBSR: Towards Lightweight Blind Super-Resolution via Discriminative Implicit Degradation Representation Learning

Supplementary Material

Sec.1 presents the ablation study of our method under *Degradation Setting 2*. Sec.2 provides implicit degradation representation (IDR) discriminative evaluation, qualitative and quantitative comparison of different methods on unseen degradations. Sec.3 showcases the recovery effects of various methods across multiple degradation scenarios.

1. Additional Ablation Study

To comprehensively validate the effectiveness of the proposed method, we further analyze the effects of each component under *Degradation Setting 2*. We select nine anisotropic Gaussian blur kernels. For each kernel, we show the average PSNR on B100 benchmark [14] under degradation combinations with noise levels of 5 and 10.

1.1. Core Components for Training

Similarly, we primarily analyze the effect of degradation reference prior (DRP), contrastive learning (CL), and the number of positive samples on SR performance.

1) Effect of DRP and CL. These two are used to enhance the discriminability of IDRs. The results are shown in Table 1. We also build four models: T1 is the baseline model without DRP and CL. T2 incorporates DRP and achieves an average PSNR improvement over T1 of 0.20 dB across different degradation conditions. T3 introduces CL and achieves an average PSNR improvement over T1 of 0.17 dB across different blur kernels. By combining DRP and CL, our method (T4) achieves 0.26 dB improvement in average PSNR on all blur kernels compared to T1. The above results indicate that DRP and CL are crucial for training the IDR-estimator, and they are compatible.

2) Impact of Positive Sample Number. To further verify the impact of the number of positive samples D on the SR performance, we conduct experimental analysis under four different anisotropic Gaussian blur kernels. The results are shown in Fig.1. Consistent with the conclusion under the *Degradation Setting 1*, our method achieves the best balance between performance and training computational cost when the number of positive samples D is set to 4.

1.2. Core Components of IDR-AM

For IDR-AM, we primarily validate the effectiveness of the IDR Adaptation Block (IDR-AB) and the IDR Correction Block (IDR-CB). The results are presented in Table 2.

1) Effect of IDR-AB. There are two degradation modulation branches: channel-wise ($\widehat{R}_C$) and spatial-wise ($\widehat{R}_S$). M1 represents the baseline model without any modulation
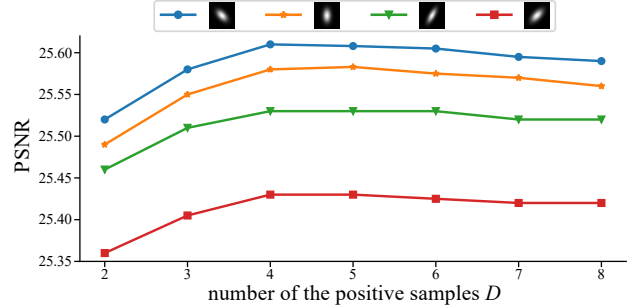

Figure 1. The effect of different numbers of positive samples.

branch. Compared to M1, by adding spatial-wise modulation (M2) or channel-wise modulation (M3), the average PSNR on all blur kernels are 0.75 dB and 0.77 dB higher than that of M1, respectively. Furthermore, by applying both spatial- and channel-wise modulation, the PSNR results on all blur kernels can be further improved compared to M2 and M3. The above results show the effectiveness and complementarity of the two modulation branches.

2) Effect of IDR-CB. Firstly, we obtain M5 by removing the IDR-CB from M4 (ours). It can be observed that the average PSNR of M5 is 0.07 dB lower than M4 on all blur kernels, demonstrating the promoting effect of IDR-CB on SR performance. Secondly, we add random values ranging from 0 to 1 to the output of the IDR-estimator for both the M4 and M5 to simulate incorrect IDR inputs, and define the results as M4- (with IDR-CB) and M5- (without IDR-CB), respectively. We can see that M4- achieves higher PSNR values than M5- across all degradation scenarios, demonstrating that the IDR-CB can effectively mitigate the adverse effects of incorrect degradation estimation.

2. Out-of-distribution (OOD) Evaluation

To validate the generalizability, we evaluate the performance of all methods in degradation scenarios outside the training range, including three experimental perspectives: IDR distribution, quantitative and qualitative evaluation.

2.1. The OOD evaluations in Degradation Setting 1

Under *Degradation Setting 1*, we compare the SR performance of different methods from both quantitative and qualitative perspectives. The results are as follows.

Quantitative evaluation. We use three different isotropic blur kernel widths {4.8, 5.0, 5.2} to evaluate the SR performance of various methods across four classic benchmarks. The comparison results with CDFormer$_S$ [12], DSAT [11],
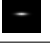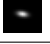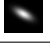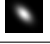
Teacher	DRP	CL									
T1			26.28	26.20	25.52	25.37	25.33	25.28	25.17	24.91	24.58
T2	✓		26.47	26.43	25.73	25.56	25.52	25.47	25.36	25.10	24.79
T3		✓	26.49	26.40	25.74	25.51	25.50	25.44	25.31	24.99	24.77
T4(Ours)	✓	✓	**26.53**	**26.46**	**25.77**	**25.61**	**25.58**	**25.53**	**25.43**	**25.15**	**24.86**

Table 1. The effect of different training framework designs on the average PSNR for noise levels of 5 and 10 under nine different anisotropic blur kernels in *Degradation Setting 2*.
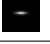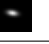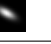
Method	$\widehat{R}_S$	$\widehat{R}_C$	IDR-CB									
M1				25.82	25.64	24.87	24.82	24.89	24.75	24.63	24.36	24.09
M2	✓		✓	26.49	26.43	25.74	25.59	25.55	25.48	25.41	25.11	24.84
M3		✓	✓	26.51	26.44	25.74	25.60	25.57	25.51	25.42	25.13	24.85
M4(Ours)	✓	✓	✓	**26.53**	**26.46**	**25.77**	**25.61**	**25.58**	**25.53**	**25.43**	**25.15**	**24.86**
M5	✓	✓		26.47	26.40	25.71	25.57	25.50	25.45	25.32	25.11	24.75
M4-	M4 with error IDRs			26.24	26.19	25.20	25.20	25.11	25.02	24.90	24.33	23.82
M5-	M5 with error IDRs			26.20	26.18	25.18	25.02	24.98	24.89	24.69	24.23	23.72

Table 2. The effect of different IDR-AM designs on the average PSNR for noise levels of 5 and 10 under nine different anisotropic blur kernels in *Degradation Setting 2*.

Method	Param.	Dataset	Set5			Set14			B100			Urban100		
		Kernel width	4.8	5.0	5.2	4.8	5.0	5.2	4.8	5.0	5.2	4.8	5.0	5.2
DAN	4.3M	CNN	**25.95**	**25.36**	**24.93**	24.24	23.84	23.47	<u>24.52</u>	<u>24.23</u>	**23.98**	21.73	<u>21.34</u>	21.04
DASR	5.8M	CNN	25.77	25.23	24.83	24.24	23.85	**23.51**	24.45	24.18	<u>23.95</u>	21.66	21.32	<u>21.05</u>
MRDA	5.8M	CNN	<u>25.90</u>	25.30	24.84	24.10	23.70	23.35	24.46	24.13	23.86	21.64	21.23	20.93
KDSR	5.8M	CNN	<u>25.90</u>	<u>25.31</u>	24.84	**24.38**	**23.90**	<u>23.50</u>	<u>24.52</u>	24.20	23.92	<u>21.77</u>	21.33	21.00
DSAT	15.6M	Transformer	25.54	25.07	24.71	24.08	23.71	23.40	24.51	**24.24**	**23.98**	21.63	21.29	21.00
CDFormer$_S$	11.9M	Transformer	25.71	25.18	24.77	24.10	23.72	23.38	24.41	24.13	23.89	21.56	21.21	20.92
LightBSR	**3.1M**	CNN	**25.95**	**25.36**	<u>24.92</u>	<u>24.30</u>	<u>23.88</u>	**23.51**	**24.54**	**24.24**	**23.98**	**21.83**	**21.40**	**21.08**

Table 3. Quantitative comparison of PSNR metric for different methods under unseen degradations on ×4 SR. The best and second-best results are highlighted in red and blue, respectively.

KDSR [18], MRDA [17], DASR [16], and DAN [7] are presented in Table 3. It can be seen that our proposed LightBSR achieves the best or second-best results across all degradation scenarios while maintaining the minimum number of parameters among all competitors.

Qualitative evaluation. We also present the visual SR results of these methods on unseen degradations. The comparison results are shown in Fig.3. It can be observed that even when facing unseen degradation settings, LightBSR is capable of clearly and accurately restoring texture details, demonstrating the strong generalizability of our method.

2.2. The OOD evaluations in Degradation Setting 2

Under more complex *Degradation Setting 2*, we focus on evaluating the discriminative ability of the IDR space learned by each method for OOD degradation patterns.

Quality of IDRs. We apply four different unseen anisotropic blur kernels on the B100 benchmark [14] to generate LR images, which are then input to DASR [16], MRDA [17], KDSR [18], DSAT [11], CDFormer$_S$ [12] and LightBSR. Comparing the IDR distributions of various methods in Fig.2, it can be observed that: 1) CDFormer$_S$ struggles to differentiate different unseen degradations, demonstrating

that diffusion-based estimator still needs optimization. 2) DSAT and DASR cannot deal with unknown degradation, indicating that only CL-based training framework cannot achieve good IDR generalization. 3) KDSR, MRDA and LightBSR all show the discriminability for various unseen degradations, with the latter two showing significant advantages. These three methods all adopt the idea of KD and introduce degradation priors or multi-stage pipelines during training, showing that sophisticated IDR modeling is crucial for improving IDR generalization.

3. Additional Visual Results

Visual Comparison in *Degradation Setting 1*. We present the ×4 SR results of different models under *Degradation Setting 1* in Fig.4, Fig.5, and Fig.6. The competitors include IDE-based methods CDFormer$_S$ [12], DSAT [11], KDSR [18], MRDA [17] and DASR [16], and EDE-based methods IKC [4] and DAN [7]. Compared to these methods, our method achieves superior visual restoration, producing clearer text, architectural details, and animal textures.

Visual Comparison in *Degradation Setting 2*. We provide the ×4 SR results under *Degradation Setting 2* in Fig.7 and Fig.8. Considering that IKC [4], DAN [7] and DCLS
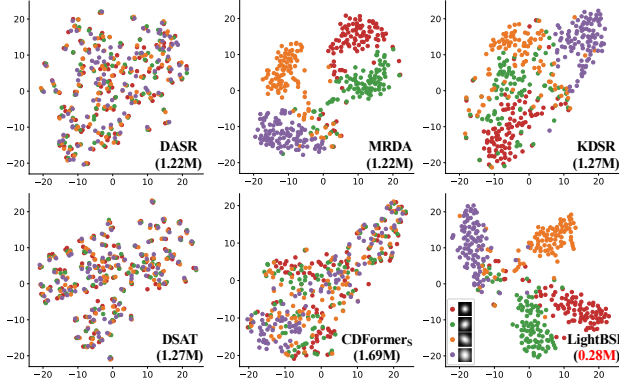
Figure 2. The t-SNE [15] plots of IDR distributions on the B100 benchmark [14]. Four different unseen anisotropic blur kernels are chosen under *Degradation Setting 2*, with the noise level set to 4.

[13] are unable to denoise images, we first apply the DnCNN [20] method as a denoising preprocessing step for these approaches. Compared to these methods, LightBSR produces clearer textures and more visually acceptable results under complex degradation scenarios.

Visual Comparison in Real Degradation Scenario. Finally, we also provide some ×4 SR results under real degradations, using the RealWorld38 [10] dataset. The visual comparison of different models trained under *Degradation Setting 2* is shown in Fig.9. It can be observed that even for real degradations, our method also achieves satisfactory results in terms of detail and texture restoration.

4. Related Work

The key to BSR is to use a learnable estimator to extract degradation information from LR images instead of manually setting degradation parameters [19, 21], to guide image reconstruction. Early BSR methods explicitly predict degradation parameters, i.e. EDE-BSR task. IKC [4] iteratively refined the estimator by using generated SR images until the satisfactory SR result is achieved. DAN [7] introduced a two-branch network that predicts the blur kernel and SR image in parallel, alternately updating blur kernel estimation and SR reconstruction. DCLS [13] incorporated a deep constrained least square filtering module, adaptively producing deblurred features from the LR image. Despite remarkable progress, this kind of method typically requires numerous iterations to compute degradation parameters, making it complex and time-consuming. To solve this problem, some works focus on the implicit modeling of degradation, called IDE-BSR, with a research emphasis on learning a latent representation space for various degradations and integrating implicit degradation representation with LR features. DASR [16] used contrastive learning [5] for the first time to model implicit representation of different degradations by learning the similarities and differences between samples. IDMBSR

[22] incorporated the kernel width and noise level as weakly supervised signals to guide the implicit estimator training. MRDA [17] used meta-learning [3] and a multi-stage strategy to implicitly learn degradation representations. KDSR [18] used the knowledge distillation (KD) [1, 6, 8] for the first time to learn the IDR estimator, where HR images are used to assist in teacher training, with the learned knowledge transferred to the student for degradation estimation during inference. Recently, both DSAT [11] and CDFormer [12] have adopted the design of building large SR networks by stacking Transformer blocks [2, 9] to achieve good effect, but over-complex models also limit their application. Compared with latest methods that improve effect by expanding model parameters, our goal is to achieve a high-performance and low complexity BSR model by strengthening the discriminability of implicit degradation space.

References

[1] Romero Adriana, Ballas Nicolas, K Samira Ebrahimi, Chassang Antoine, Gatta Carlo, and B Yoshua. Fitnets: Hints for thin deep nets. *ICLR*, 2:3, 2015. 3

[2] Zheng Chen, Yulun Zhang, Jinjin Gu, Linghe Kong, Xiaokang Yang, and Fisher Yu. Dual aggregation transformer for image super-resolution. In *ICCV*, 2023. 3

[3] Chelsea Finn, Pieter Abbeel, and Sergey Levine. Model-agnostic meta-learning for fast adaptation of deep networks. In *ICML*, 2017. 3

[4] Jinjin Gu, Hannan Lu, Wangmeng Zuo, and Chao Dong. Blind super-resolution with iterative kernel correction. In *CVPR*, 2019. 2, 3

[5] Kaiming He, Haoqi Fan, Yuxin Wu, Saining Xie, and Ross Girshick. Momentum contrast for unsupervised visual representation learning. In *CVPR*, 2020. 3

[6] Geoffrey Hinton, Oriol Vinyals, and Jeff Dean. Distilling the knowledge in a neural network. *arXiv preprint arXiv:1503.02531*, 2015. 3

[7] Yan Huang, Shang Li, Liang Wang, Tieniu Tan, et al. Unfolding the alternating optimization for blind super resolution. In *NeurIPS*, 2020. 2, 3

[8] Guanzhou Ke, Bo Wang, Xiaoli Wang, and Shengfeng He. Rethinking multi-view representation learning via distilled disentangling. In *CVPR*, pages 26774–26783, 2024. 3

[9] Jingyun Liang, Jiezhang Cao, Guolei Sun, Kai Zhang, Luc Van Gool, and Radu Timofte. Swinir: Image restoration using swin transformer. In *ICCV*, 2021. 3

[10] Jie Liang, Hui Zeng, and Lei Zhang. Efficient and degradation-adaptive network for real-world image super-resolution. In *ECCV*, 2022. 3

[11] Qingguo Liu, Pan Gao, Kang Han, Ningzhong Liu, and Wei Xiang. Degradation-aware self-attention based transformer for blind image super-resolution. *TMM*, 2024. 1, 2, 3

[12] Qingguo Liu, Chenyi Zhuang, Pan Gao, and Jie Qin. Cdformer: When degradation prediction embraces diffusion model for blind image super-resolution. In *CVPR*, 2024. 1, 2, 3

[13] Ziwei Luo, Haibin Huang, Lei Yu, Youwei Li, Haoqiang Fan, and Shuaicheng Liu. Deep constrained least squares for blind image super-resolution. In *CVPR*, 2022. 3

[14] David Martin, Charless Fowlkes, Doron Tal, and Jitendra Malik. A database of human segmented natural images and its application to evaluating segmentation algorithms and measuring ecological statistics. In *ICCV*, 2001. 1, 2, 3

[15] Laurens Van der Maaten and Geoffrey Hinton. Visualizing data using t-sne. *Journal of machine learning research*, 9(11), 2008. 3

[16] Longguang Wang, Yingqian Wang, Xiaoyu Dong, Qingyu Xu, Jungang Yang, Wei An, and Yulan Guo. Unsupervised degradation representation learning for blind super-resolution. In *CVPR*, 2021. 2, 3

[17] Bin Xia, Yapeng Tian, Yulun Zhang, Yucheng Hang, Wen-ming Yang, and Qingmin Liao. Meta-learning-based degradation representation for blind super-resolution. *IEEE Trans. Image Process.*, 32:3383–3396, 2023. 2, 3

[18] Bin Xia, Yulun Zhang, Yitong Wang, Yapeng Tian, Wenming Yang, Radu Timofte, and Luc Van Gool. Knowledge distillation based degradation estimation for blind super-resolution. In *ICLR*, 2023. 2, 3

[19] Yu-Syuan Xu, Shou-Yao Roy Tseng, Yu Tseng, Hsien-Kai Kuo, and Yi-Min Tsai. Unified dynamic convolutional network for super-resolution with variational degradations. In *CVPR*, 2020. 3

[20] Kai Zhang, Wangmeng Zuo, Yunjin Chen, Deyu Meng, and Lei Zhang. Beyond a gaussian denoiser: Residual learning of deep cnn for image denoising. *IEEE Trans. Image Process.*, 26(7):3142–3155, 2017. 3

[21] Kai Zhang, Wangmeng Zuo, and Lei Zhang. Learning a single convolutional super-resolution network for multiple degradations. In *CVPR*, 2018. 3

[22] Yongfei Zhang, Ling Dong, Hong Yang, Linbo Qing, Xiaohai He, and Honggang Chen. Weakly-supervised contrastive learning-based implicit degradation modeling for blind image super-resolution. *KBS*, 249:108984, 2022. 3
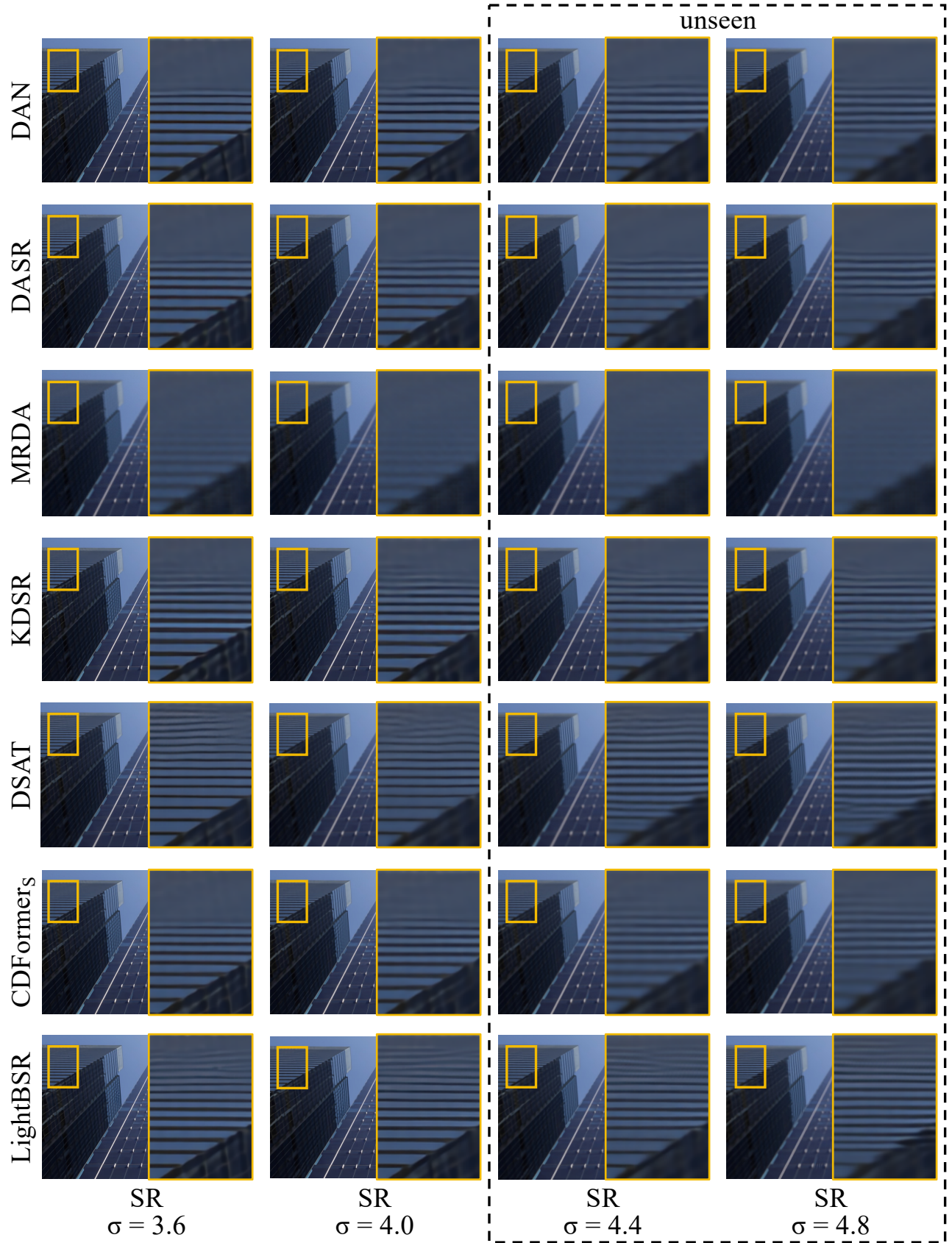
Figure 3. ×4 SR visual results of various methods on the "img_033" of the Urban100 under unseen degradation settings. Zoom in to view additional details.
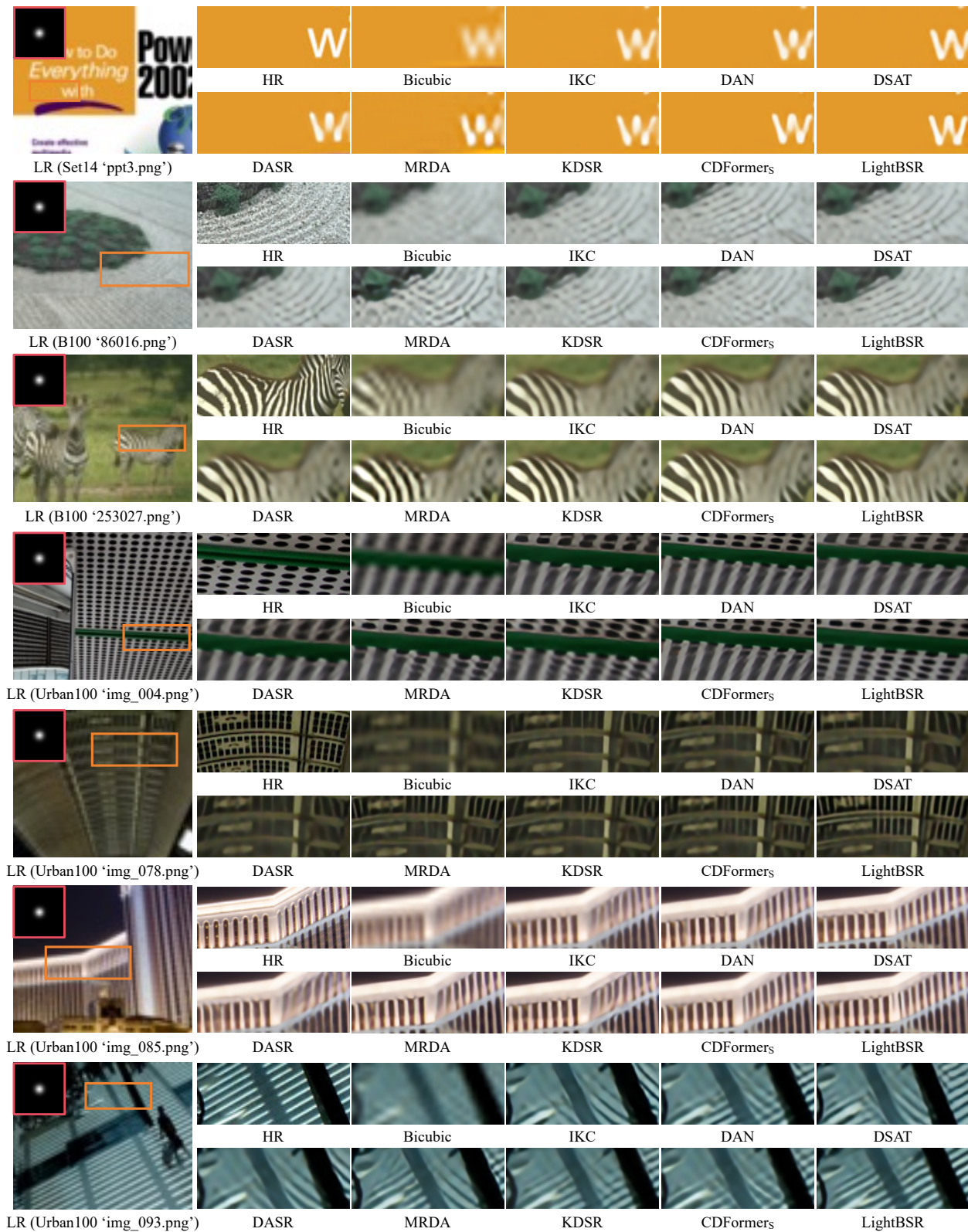
Figure 4. ×4 SR results for isotropic Gaussian blur kernel width 1.2 on Set14, B100 and Urban100 benchmarks.
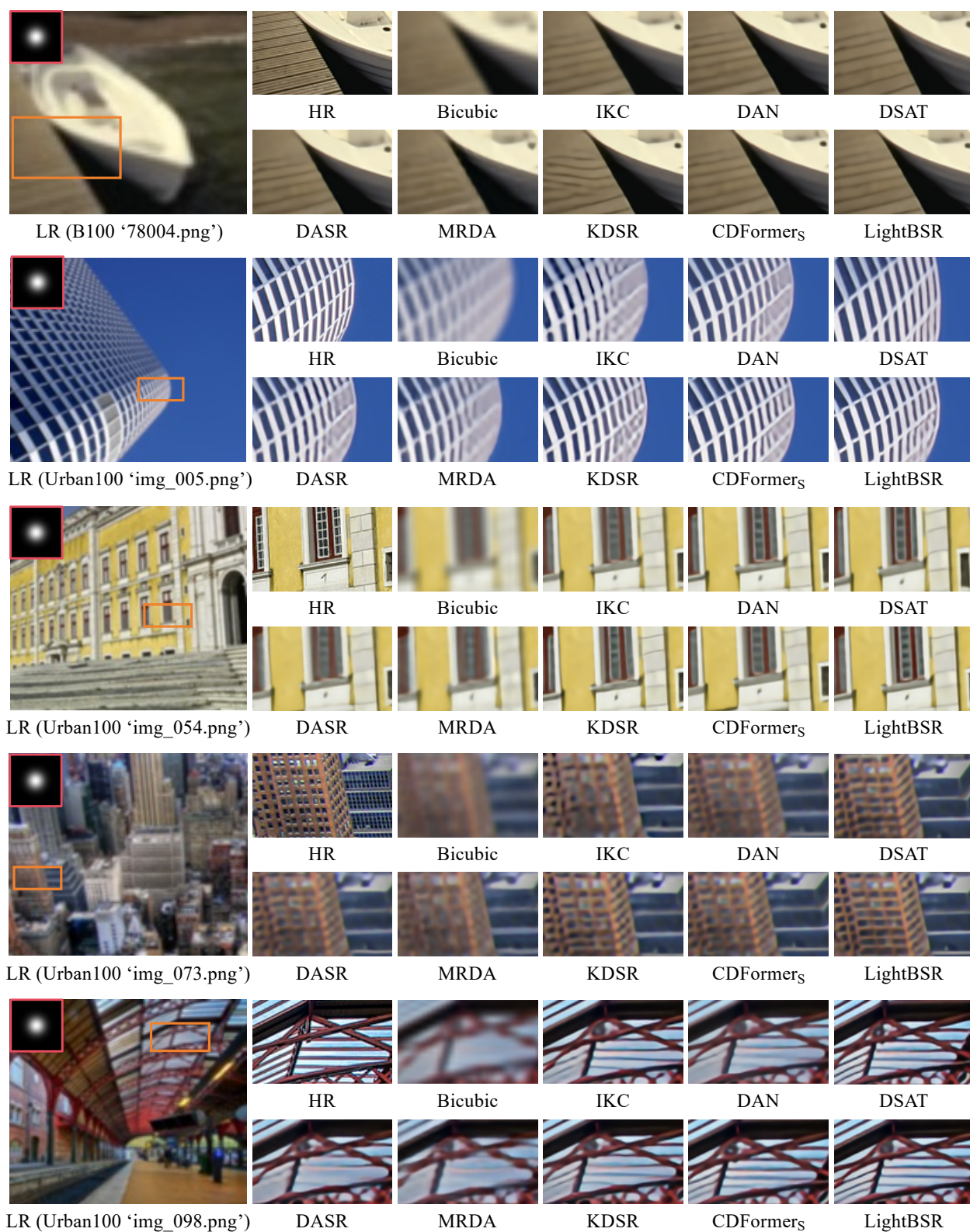
Figure 5. ×4 SR results for isotropic Gaussian blur kernel width 2.4 on B100 and Urban100 benchmarks.

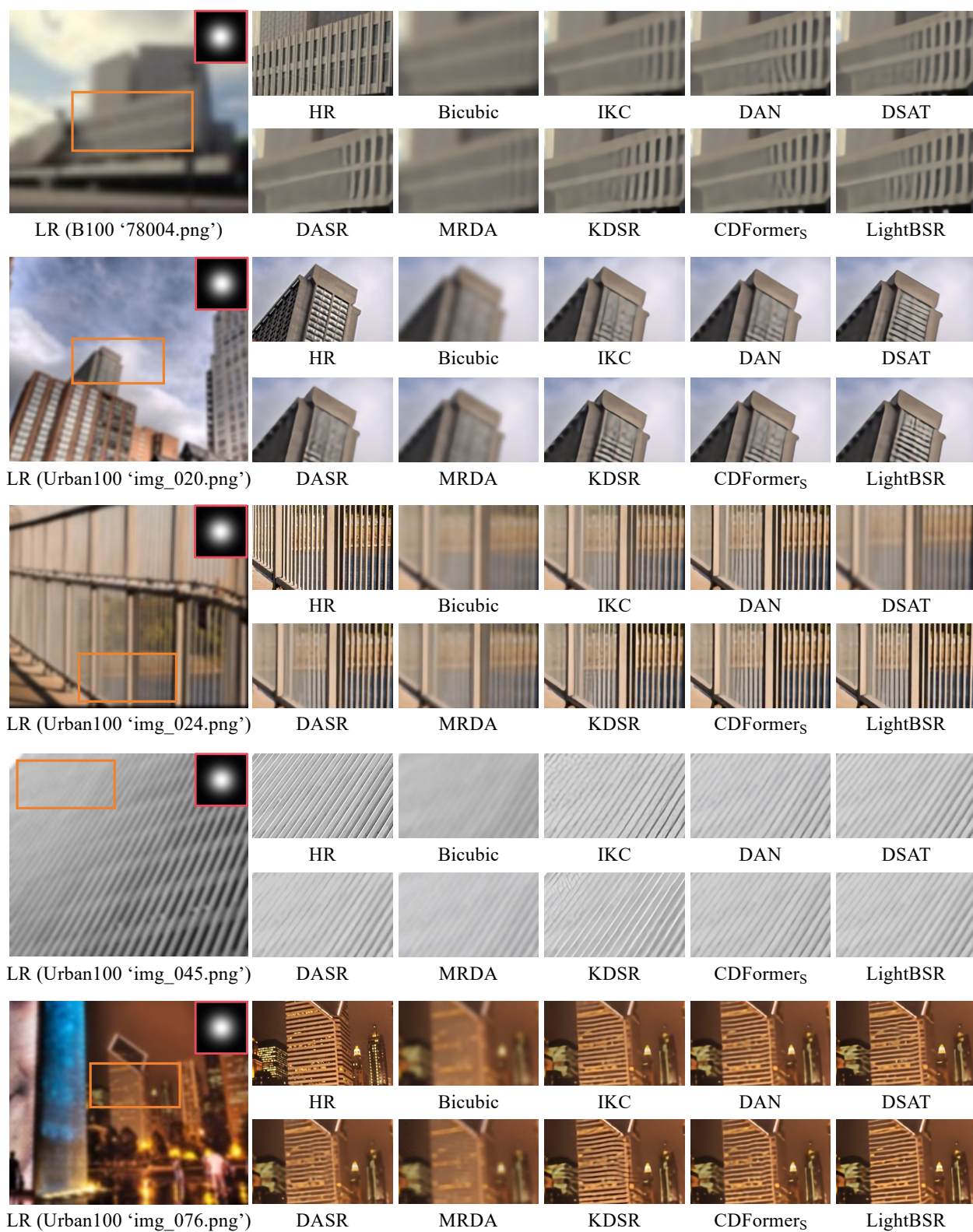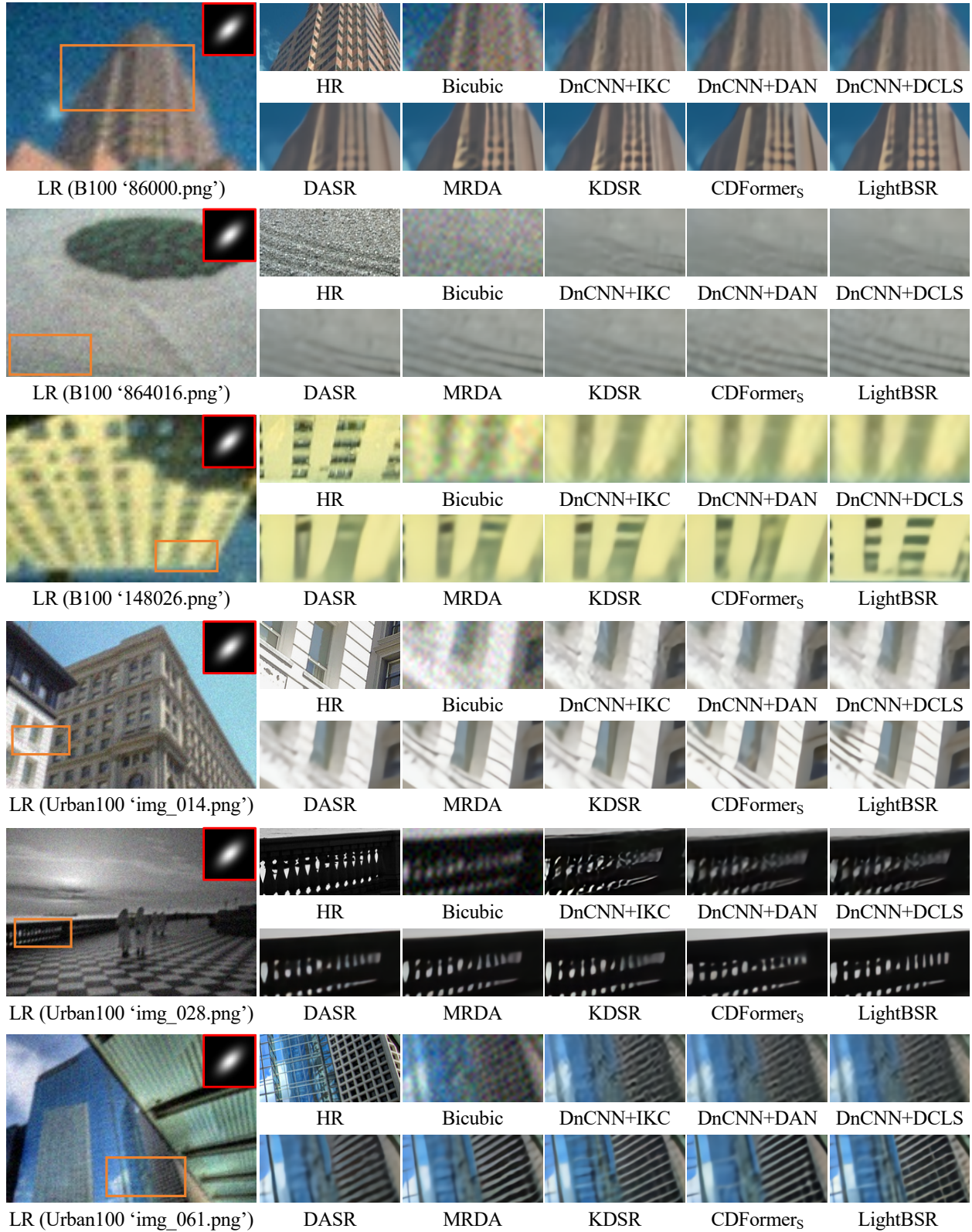Figure 6. ×4 SR results for isotropic Gaussian blur kernel width 3.6 on B100 and Urban100 benchmarks.

Figure 7. ×4 SR results on B100 and Urban100 benchmarks under an anisotropic Gaussian blur kernel with a noise level of 5.

The labels appearing within the figure, row by row:

LR (B100 '108005.png') — HR, Bicubic, DnCNN+IKC, DnCNN+DAN, DnCNN+DCLS — DASR, MRDA, KDSR, CDFormer$_S$, LightBSR

LR (B100 '134035.png') — HR, Bicubic, DnCNN+IKC, DnCNN+DAN, DnCNN+DCLS — DASR, MRDA, KDSR, CDFormer$_S$, LightBSR

LR (B100 '223061.png') — HR, Bicubic, DnCNN+IKC, DnCNN+DAN, DnCNN+DCLS — DASR, MRDA, KDSR, CDFormer$_S$, LightBSR

LR (Urban100 'img_019.png') — HR, Bicubic, DnCNN+IKC, DnCNN+DAN, DnCNN+DCLS — DASR, MRDA, KDSR, CDFormer$_S$, LightBSR

LR (Urban100 'img_050.png') — HR, Bicubic, DnCNN+IKC, DnCNN+DAN, DnCNN+DCLS — DASR, MRDA, KDSR, CDFormer$_S$, LightBSR

LR (Urban100 'img_053.png') — HR, Bicubic, DnCNN+IKC, DnCNN+DAN, DnCNN+DCLS — DASR, MRDA, KDSR, CDFormer$_S$, LightBSR

Figure 8. ×4 SR results on B100 and Urban100 benchmarks under an anisotropic Gaussian blur kernel with a noise level of 10.

RealWorld38 'img006.png'   Bicubic   DASR   MRDA   KDSR   CDFormer$_S$ LightBSR

RealWorld38 'pattern.png'   Bicubic   DASR   MRDA   KDSR   CDFormer$_S$ LightBSR

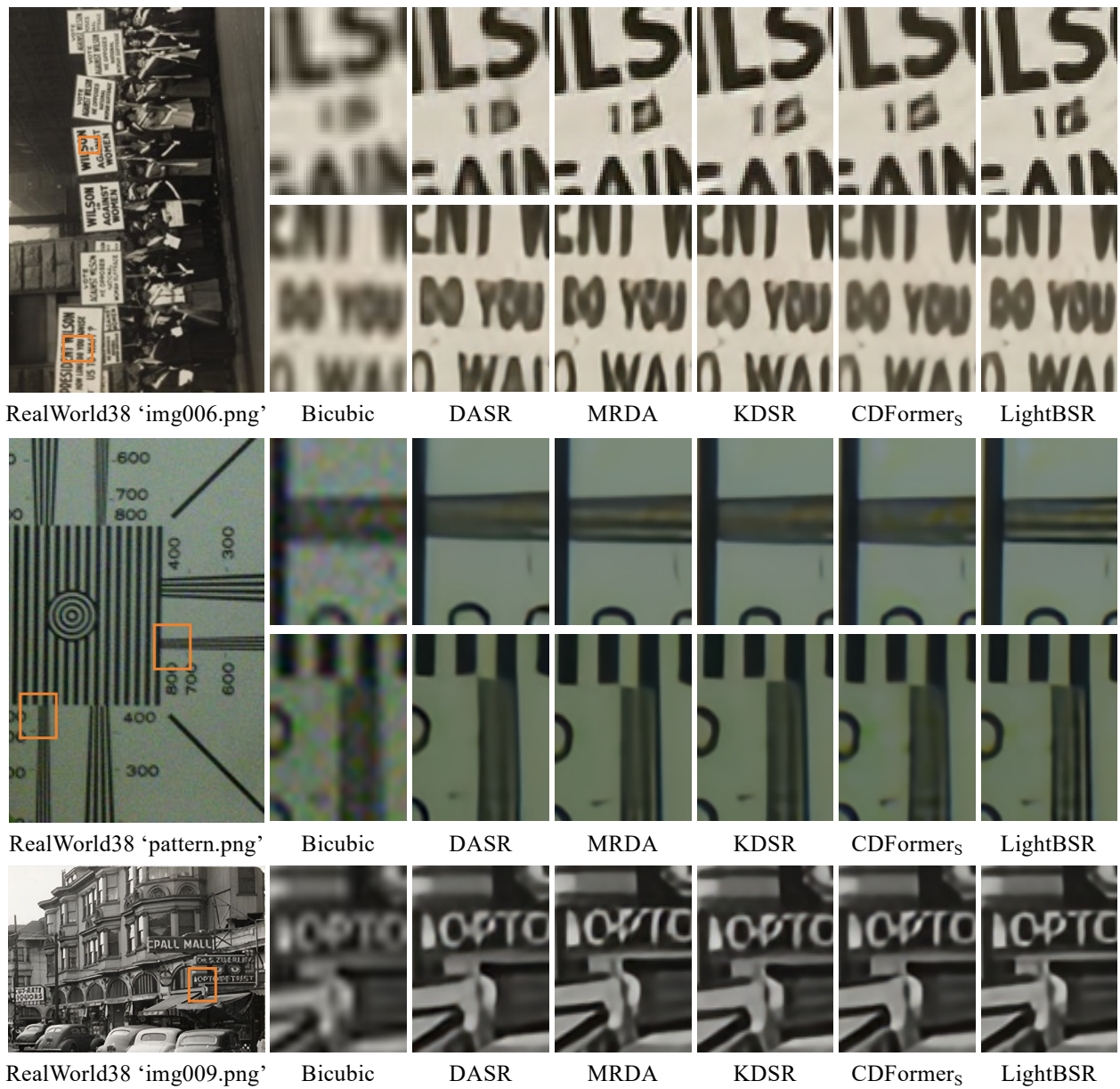RealWorld38 'img009.png'   Bicubic   DASR   MRDA   KDSR   CDFormer$_S$ LightBSR

Figure 9. ×4 SR results on the RealWorld38 benchmark.